13th International Symposium on Particle Image Velocimetry – ISPIV 2019
Munich, Germany, July 22-24, 2019

Toward automated 3D PTV for microfluidics

Massimiliano Rossi[1]* **and Rune Barnkob**[2]

[1] Department of Physics, Technical University of Denmark, Kongens Lyngby, Denmark

[2] Heinz-Nixdorf-Chair of Biomedical Electronics, Department of Electrical and Computer Engineering, Technical University of Munich, Munich, Germany

* rossi@fysik.dtu.dk

Abstract

The increasing use of microfluidics in biomedical applications is demanding more precise and continuous measurements of microfluidic flows and suspended microparticles and cells. One approach, promising for being widely-used in microfluidics, is the General Defocusing Particle Tracking (GDPT) as it is suitable for non-expert use and only requires equipment standard in a microfluidic laboratory. In this work we present a strategy for performing GDPT in a more automated manner, which is especially suitable for applications where real-time feedback control is needed. We demonstrate the strategy by simulating real-time experiments by use of synthetic images. The experiments consist in the automatic identification of the focusing time of particles in an acoustofluidic device. The simulation were performed on a conventional laptop and showed that it was possible to successfully achieve this task with a temporal resolution of 1 sec, on different type of images (darkfield and brightfield), and that the approach is not sensitive to background or illumination fluctuations.

1 Introduction

The recent advancements in microfluidic devices, specially in fields like biology or medicine, require more and more precise and continuous measurements of microfluidic flow fields. In particular, two main needs are emerging in this domain: 3D-PTV tools that can be effectively operated by non-expert users like biologists or physicians, and automated methods suitable for active force and flow control (e.g. to allow single-cell manipulation via acoustofluidics). Since the first application of microscopic PIV by Santiago et al. (1998), about two decades ago, several methods have been proposed to track position and velocity of particles in microfluidics, both in 2D and 3D, using very different principles such as defocusing, astigmatism, evanescent waves, holography and so on [Raffel et al. (2018)]. However, most of these methods requires complex calibration procedures as well as experienced users to properly perform a measurement and are not suitable for quick or real-time applications [Cierpka and Kähler (2012)].

One method that has the potential to meet both the above mentioned needs is the General Defocusing Particle Tracking (GDPT) proposed by Barnkob et al. (2015), see Fig. 1. The only requirements for performing GDPT measurements is to have an optical system with sufficiently small depth of field (particle images must have different shape depending on their depth position) and a stack of calibration images taken at known depth positions. Both requirements are normally fulfilled in microfluidics applications, where large magnification objective lens are used and calibration stacks can easily be obtained just by moving the focus of the microscope. Furthermore, GDPT can indifferently be used on brightfield, darkfield, or fluorescent images as long as the image contrast is sufficiently high and outliers are automatically rejected based on a single similarity parameter that evaluate how well a target image is matched to the calibration image stack. Therefore, and due to its simplicity, GDPT is receiving an increasing interest in microfluidics and lab-on-a-chip communities, such as within the acoustic manipulation of microparticles, where information about the three-dimensional acoustophoretic behavior is crucial to further development [Karlsen et al. (2018); Qiu et al. (2019)].

In this work, we present a new strategy to perform GDPT measurements in a more automated fashion by using cross-correlation rather than segmentation for the detection of target particles. The strategy is tested with several simulated real-time acoustofluidics experiments, created using analytical predictions of particle trajectories in acoustofluidic devices [Muller et al. (2013)] and synthetic images of particles in the

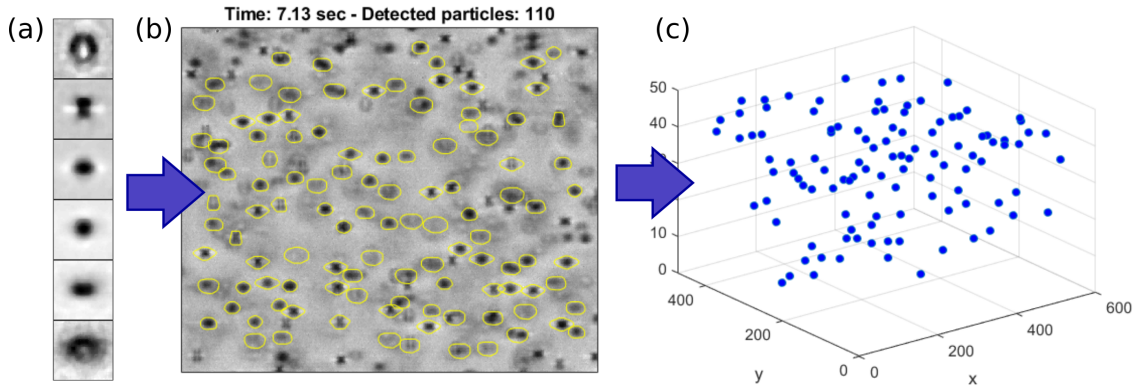

Figure 1: An example of 3D particle tracking performed by GDPT using a conventional microscope with brightfield illumination and a cylindrical lens introduced in front of the camera sensor. (a) The stack of reference calibration images of a spherical particle at known depth positions. (b) The raw image of the particles in the flow. The yellow contours indicate particles with identified 3D positions. (c) The resulting 3D particle positions corresponding to the identified particles.

flow generated with MicroSIG, a recently developed synthetic image generator for defocused and astigmatic particle images [Rossi (2019)].

2 Fast and user-free General Defocusing Particle Tracking

The basic concept of GDPT includes a look-up table that maps defocused or astigmatic particle images with their respective z position (calibration stack) and a function to compare the similarity between a target particle image and the reference particle images in the stack. In Barnkob et al. (2015) and in this work we used for this purpose the normalized cross-correlation [Lewis (1995)] between the target and calibration images and take as similarity coefficient the maximum value, referred to as C_m (see Fig. 2 (d)). C_m values go from 0 to 1, with 1 corresponding to a perfect match between target and calibration image. The conventional approach for GDPT measurements used in Barnkob et al. (2015) consists of a segmentation step to identify candidate particles images, a guessing step where a rough z position is determined from a subset of the calibration stack, and a refinement step where a walking procedure is used to refine the z position. This procedure is very accurate, however, it is relatively slow since it needs to compute a large number of cross-correlations. Moreover, the segmentation procedure must be optimized for each image type and fails if the background or the illumination is not uniform, therefore a pre-processing step is often required.

In this work, we propose a new algorithm to perform GDPT measurements without the segmentation step and with fewer cross-correlations per image. The method is summarized in Fig. 2. First, we select a subset of N_sub calibration images from the calibration stack. For each image in the calibration stack, we calculate an "expected" C_m profile by performing a normalized cross-correlation with the images in the subset (Fig. 2 (a)). This gives a mapping of expected results that will be used during the evaluation for fast identification of z positions. Second, to evaluate the target image, we first perform normalized cross-correlations between the image and the N_sub calibration images in the subset (Fig. 2 (b)). The correlation maps have values between 0 and 1 and peak values are located in the center of the particle images with shape similar to the corresponding calibration image. From this approach we have two significant advantages: (1) We can identify candidate particles by looking at the local peaks with magnitude larger than a certain threshold (normally 0.5), regardless of the shape and type of images (fluorescent, brightfield, with non-uniform illumination, etc.). (2) For each identified target particle, we have the in-plane position and a profile of C_m values for N_sub z-positions with no need of additional cross-correlations. Each correlation profile can now be compared with the mapping of expected C_m profiles to obtain a robust guess of the z position (Fig. 2 (c)).

With this procedure it is possible to obtain a robust and fast first guess of 3D particle positions, without a segmentation step and with fewer cross-correlations (N_sub). At this point, a refinement step, based on a walking procedure, can be applied to improve the accuracy of the measurement.

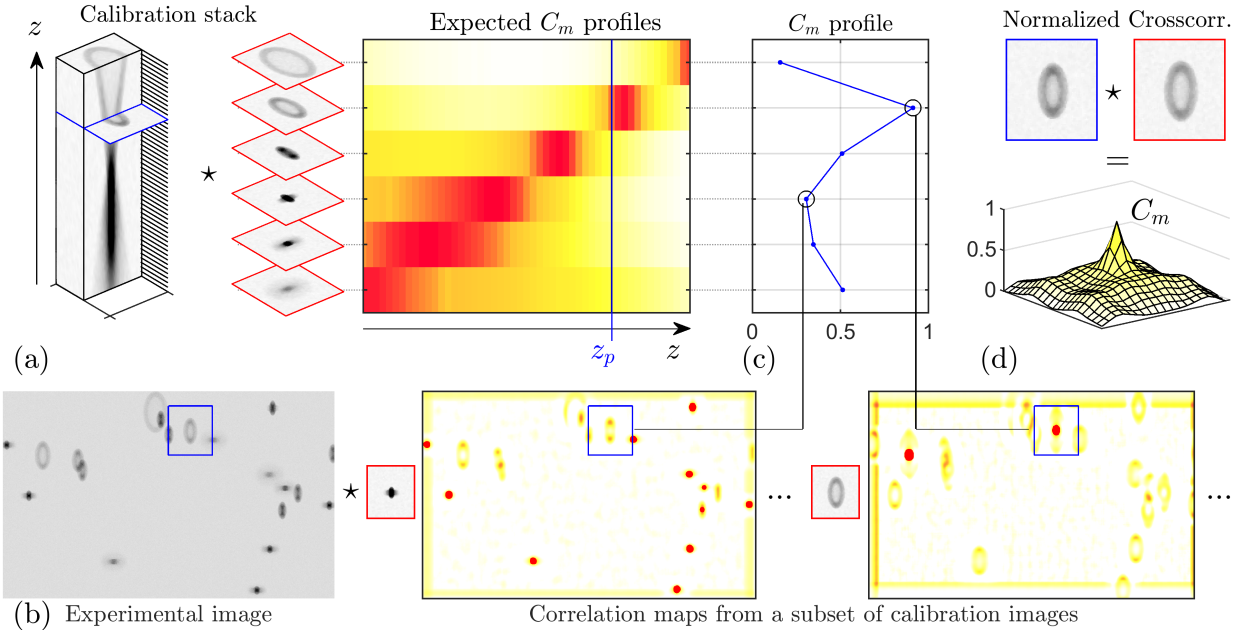

Figure 2: Evaluation method for fast GDPT. (a) During the calibration process, a subset of N_{sub} calibration images is extracted from the calibration stack and used to create a mapping of the estimated C_{m} profiles for the given subset, across the entire measurement volume height. (b) In the evaluation process, a normalized cross-correlation between the experimental image and the subset of calibration images is performed, obtaining N_{sub} correlation maps. From the maps (with values between 0 and 1), candidate particles are extracted and for each candidate the C_{m} profile is calculated (c). The z-coordinate is identified from the comparison between the measured C_{m} profile and the expected C_{m} profiles. (d) Example of normalized cross-correlation: the C_{m} value represents the (local) peak value of the correlation map.

3 Generation of synthetic images

The performance of the proposed GDPT approach is here tested on simulated experiments in which the experimental images are created using a Synthetic Image Generator (SIG). Specifically, we used MicroSIG, a SIG based on ray-tracing and a simplified spherical lens model to obtain realistic defocused or astigmatic particle images [Rossi (2019)]. The use of astigmatic aberration, which experimentally can be obtained

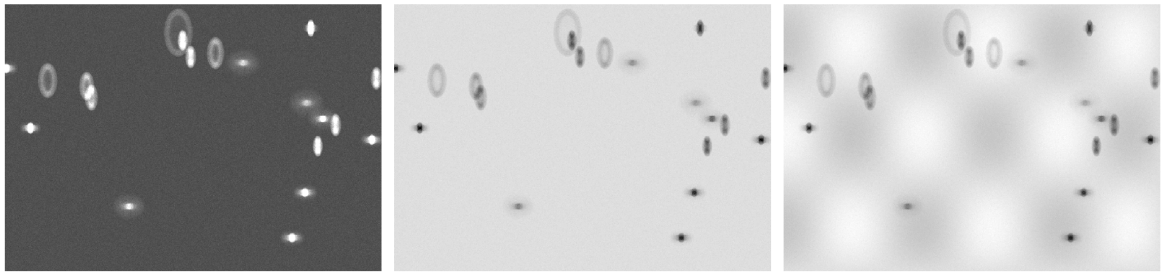

(a) Fluorescent (b) Brightfield (c) Brightfield + disturbance

Figure 3: Synthetic images used in the simulations. (a) Synthetic image of 5-µm fluorescent particles taken with a 10×/0.3 objective lens and astigmatic correction generated by the synthetic image generator MicroSIG. (b) Same image converted to a brightfield image. (c) Brightfield image disturbed with a sinusoidal intensity pattern simulating a non-homogeneous background or illumination.

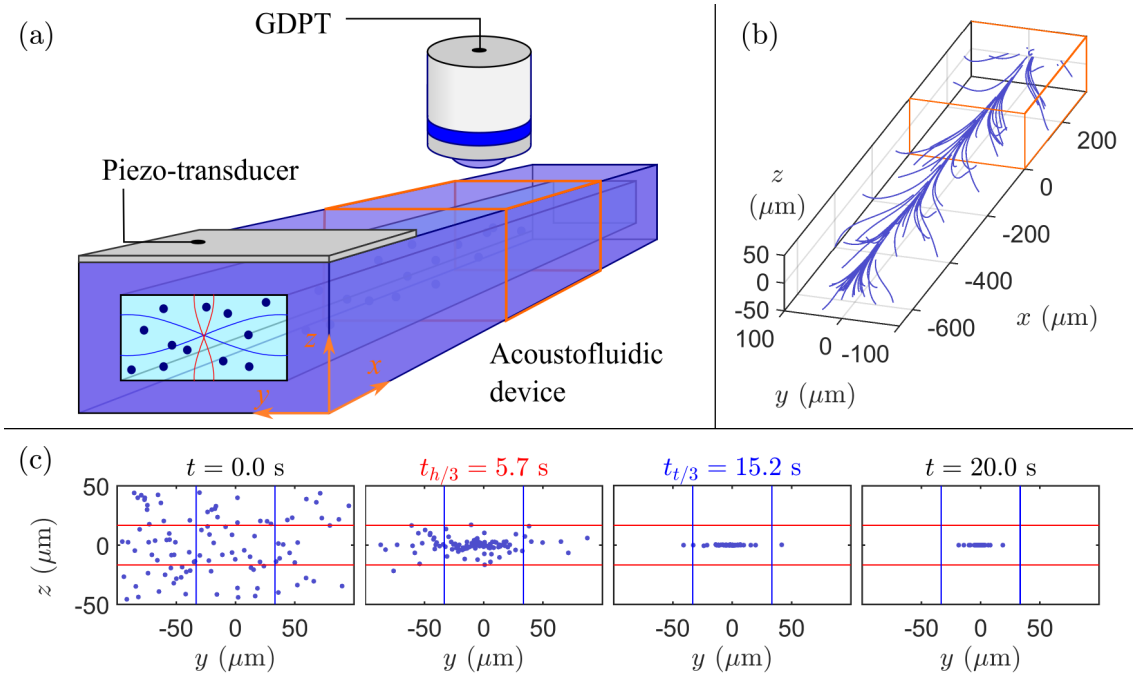

Figure 4: (a) Schematic of the simulated acoustophoretic experiment: an acoustofluidic device is used to focus particles in the center of a rectangular microchannel. Real-time GDPT measurements are used to monitor the position of the particles inside the channel and to identify the time $t_{h/3}$, when 90% of the particles are inside a vertical region of thickness $h/3$, and $t_{w/3}$, when 90% of the particles are inside a horizontal region of thickness $w/3$. (b) Simulated particle trajectories assuming a Poiseuille flow with flow rate $Q = 0.4$ µl/h and acoustic energy density $E_{ac} = 1.2$ J/m^3. (c) Cross-sectional particle position in the measurement region for different time instants.

by adding a cylindrical lens in front of the camera sensor, is used in many experimental setups to encode more efficiently the defocusing information by breaking the symmetry of defocusing patterns [Cierpka et al. (2010); Rossi and Kähler (2014)].

For the current simulations we used 5-µm-diameter spheres as tracer particles, observed with a 10×/0.3 objective lens plus astigmatic aberration on a 512×512 pixels sensor. A typical synthetic image obtained with MicroSIG is shown in Fig. 3(a), which corresponds to a classical darkfield image used in PIV setups (i.e. fluorescent particles observed with an epifluorescent microscope). Additionally, we used two other types of images: Brightfield images, obtained by inverting the values of the darkfield images (Fig. 3 (b)), and brightfield images plus an intensity disturbance, introduced to simulate non-uniform backgrounds or non-uniform illumination (Fig. 3 (c)). The disturbance consists of a 2D sinusoidal pattern.

4 Simulation of real-time GDPT of particles undergoing acoustophoresis

The simulated experiment is sketched in Fig. 4 and consists of an acoustofluidic device which focuses particles in the center of a microchannel by means of the acoustic radiation forces induced by two perpendicular standing acoustic waves. A Poiseuille flow is superimposed to simultaneously transport the particles in the stream-wise direction. The microchannel has a rectangular cross-section of width $w = 200$ µm and height $h = 100$ µm. Real-time measurements of the 3D particle positions in a section of the microchannel are taken with GDPT. The objective of the control system is to identify the two "trigger" times $t_{h/3}$ and $t_{w/3}$, when 90 % of the particles have been focused, respectively, in a vertical region of thickness $h/3$ and in a horizontal region of thickness $w/3$.

The particles are polystyrene spheres with diameter $2a = 5$ µm randomly distributed inside the channel at the beginning of each experiment. The suspending fluid is water at 25 °C. The stream-wise particle velocities are calculated from the analytical solution of a Poiseuille flow in a rectangular channel with flow

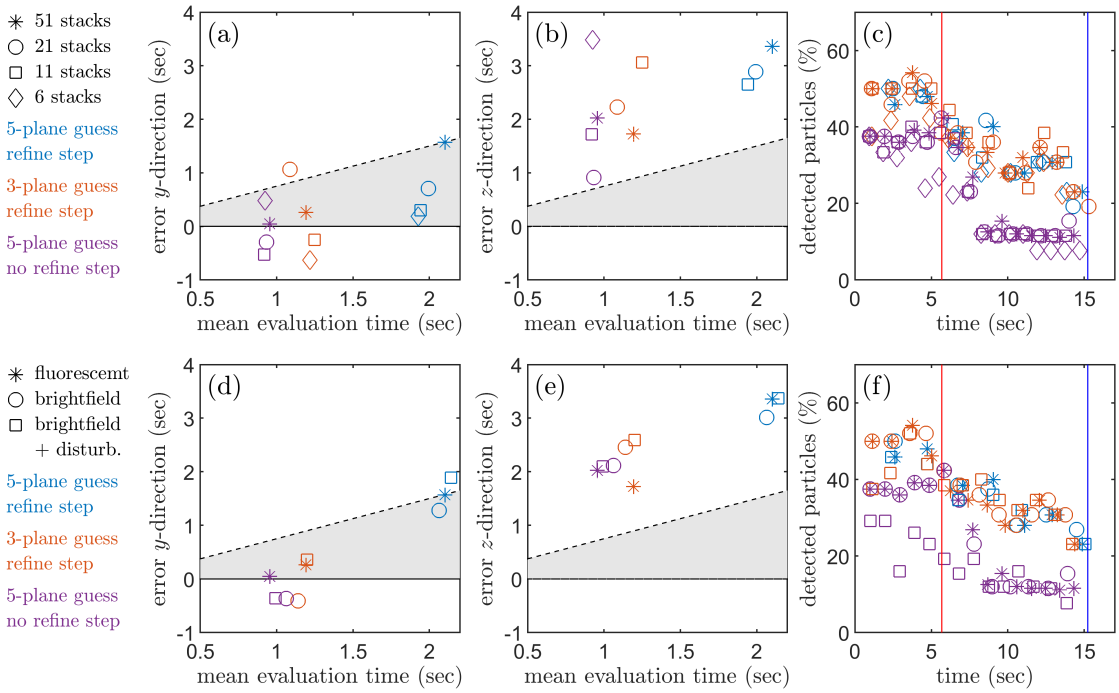

Figure 5: (a-b) Error in the determination of $t_{h/3}$ and $t_{w/3}$ versus the mean evaluation time for different settings and (c) corresponding number of valid detected particles as a function of time. The gray area represents the random delay expected for the given evaluation time. (d-e) Error in the determination of $t_{h/3}$ and $t_{w/3}$ versus the mean evaluation time for different settings and image types, and (d) corresponding number of valid detected particles as a function of time.

rate $Q = 0.4$ µl/h. The cross-sectional radiation-dominated acoustophoretic velocities are calculated using an energy density $E_{\mathrm{ac}} = 1.2$ J/m^3 and following the analytical expressions given in Muller et al. (2013)

$$u_y^{\mathrm{rad}} = u_0 \frac{a^2}{a_0^2} \sin[\pi(\frac{2y}{w} + 1)], \tag{1a}$$

$$u_z^{\mathrm{rad}} = u_0 \frac{a^2}{a_0^2} \sin[\pi(\frac{2z}{h} + 1)], \tag{1b}$$

where u_0 depends on the fluid parameters and the acoustic energy density E_{ac} of the acoustic wave, while a_0 is a function of fluid viscosity and the acoustic constrast between particle and suspending medium.

The particle trajectories determined over a time of 20 s are reported in Fig. 4. The corresponding synthetic images of the particles in the flow are obtained by means of MicroSIG as described in the previous section. An *ad hoc* Matlab routine was written to simulate real-time GDPT measurements assuming a camera frame rate of 25 fps.

4.1 Results

Results are shown in Fig. 5. There are mainly three parameters to consider for the assessment of real-time GDPT measurements: (1) the computational time of a single evaluation, (2) the accuracy of the measurement, and (3) the number of detected particles (this strongly depends on the particle concentration, since it is more difficult to process overlapping particles). Improving points (2) and (3) leads to longer computational times therefore an optimal balance must be found.

Before analyzing the results, few premises are necessary. The computational time sets also the temporal resolution of the real-time measurement, therefore a random delay error proportional to the temporal resolution is expected (gray area in the plots). Additionally, the number of valid detected particles decreases with

time as a consequence of the increasing of particle overlapping, therefore $t_{h/3}$ and $t_{w/3}$ must be guessed on a reduced set of data. Finally, the z-determination is more challenging therefore a larger error is expected in this direction.

In a first set of experiments, we tested the performance of real-time GDPT measurements on fluorescent images using different GDPT settings. Different strategies to decrease the computational time have been tested: reducing the total number N of images in the calibration stack, reducing the number N_{sub} of images in the subset of the calibration stack, removing the refinement step. In particular, we calculated the error in the determination of $t_{h/3}$ (Fig. 5 (a)) and $t_{w/3}$ (Fig. 5 (b)) as a function of the average computational time for each image, and the number of valid particles as function of time (Fig. 5 (c)). The simulations show that removing the refinement step speeds up significantly the computational time with relatively low impact on the accuracy. On the other hand, decreasing the number of images in the calibration stack minimally decrease the computational time but can cause a failure of the measurement (in Fig. 5 (b) the symbols for 6-stacks are not present for two configurations).

In a second set of experiments, we tested the performance of this approach on different types of images: fluorescent, brightfield, and brightfield with disturbance (see Fig. 3). This time we always used $N = 51$ images in the calibration stack. It should be noted that the entire measurement procedure remained exactly the same for the three types of images (except for the calibration images used, of course). The results of the simulations are presented in Fig. 5 (d-f) and show that no significant difference is observed, proving that the presented approach is suitable for different image types and is not sensitive to background fluctuations.

The simulations were performed on 512×512 images on a laptop computer with an Intel Core i5-3339Y CPU processor running at 1.50 GHz with a RAM memory of 8 GB. With this setup it was possible to achieve an evaluation time of about 1 sec, however using parallel computing and a better hardware it is certainly possible to achieve a much faster processing time using the same algorithm.

5 Conclusions

We presented a new approach to perform 3D particle tracking using GDPT that does not need preliminary pre-processing or segmentation steps. Furthermore, the presented approach needs to compute only few cross-correlations in comparison with other iterative approaches therefore is suitable for a fast evaluation time. We tested the algorithm on simulated acoustophoretic experiments, created using synthetic images and an *ad hoc* Matlab routine. The simulations show that even without refinement steps, this approach is able to perform automated control-tasks and that is not sensitive to the type of images (darkfield or brightfield) or background fluctuations.

Acknowledgements

The research leading to these results has received funding from the European Union's Horizon 2020 research and innovation programme under the Marie Sklodowska-Curie grant agreement no. 713683 (COFUNDfellowsDTU).

References

Barnkob R, Kähler CJ, and Rossi M (2015) General defocusing particle tracking. *Lab on a Chip* 15:3556–3560

Cierpka C and Kähler CJ (2012) Particle imaging techniques for volumetric three-component (3d3c) velocity measurements in microfluidics. *Journal of Visualization* 15:1–31

Cierpka C, Segura R, Hain R, and Kähler CJ (2010) A simple single camera 3c3d velocity measurement technique without errors due to depth of correlation and spatial averaging for microfluidics. *Measurement Science and Technology* 21:045401

Karlsen JT, Qiu W, Augustsson P, and Bruus H (2018) Acoustic streaming and its suppression in inhomogeneous fluids. *Physical review letters* 120:054501

Lewis JP (1995) Fast template matching. in *Vision interface*. volume 95. pages 15–19

Muller PB, Rossi M, Marin A, Barnkob R, Augustsson P, Laurell T, Kähler CJ, and Bruus H (2013) Ultrasound-induced acoustophoretic motion of microparticles in three dimensions. *Physical Review E* 88:023006

Qiu W, Karlsen JT, Bruus H, and Augustsson P (2019) Experimental characterization of acoustic streaming in gradients of density and compressibility. *Physical Review Applied* 11:024018

Raffel M, Willert CE, Scarano F, Kähler CJ, Wereley ST, and Kompenhans J (2018) *Particle Image Velocimetry*. chapter Tracer Particles, page 39. Springer. 3rd edition

Rossi M (2019) Synthetic image generator for defocusing and astigmatic PIV/PTV. *Submitted*

Rossi M and Kähler CJ (2014) Optimization of astigmatic particle tracking velocimeters. *Experiments in fluids* 55:1809

Santiago JG, Wereley ST, Meinhart CD, Beebe DJ, and Adrian RJ (1998) A particle image velocimetry system for microfluidics. *Experiments in fluids* 25:316–319